

Insert here your thesis' task.



**FACULTY
OF INFORMATION
TECHNOLOGY
CTU IN PRAGUE**

Bachelor's thesis

Gesture detector with Leap Motion sensor

Anh Tran Viet

Department of Theoretical Computer Science

Supervisor: Tomáš Nováček

June 18, 2021

Acknowledgements

THANKS (remove entirely in case you do not wish to thank anyone)

Declaration

I hereby declare that the presented thesis is my own work and that I have cited all sources of information in accordance with the Guideline for adhering to ethical principles when elaborating an academic final thesis.

I acknowledge that my thesis is subject to the rights and obligations stipulated by the Act No.121/2000 Coll., the Copyright Act, as amended, in particular that the Czech Technical University in Prague has the right to conclude a license agreement on the utilization of this thesis as a school work under the provisions of Article 60 (1) of the Act.

In Prague on June 18, 2021

.....

Czech Technical University in Prague
Faculty of Information Technology
© 2021 Anh Viet Tran. All rights reserved.

This thesis is school work as defined by Copyright Act of the Czech Republic. It has been submitted at Czech Technical University in Prague, Faculty of Information Technology. The thesis is protected by the Copyright Act and its usage without author's permission is prohibited (with exceptions defined by the Copyright Act).

Citation of this thesis

Tran, Anh Viet. *Gesture detector with Leap Motion sensor*. Bachelor's thesis. Czech Technical University in Prague, Faculty of Information Technology, 2021.

Abstrakt

V několika větách shrňte obsah a přínos této práce v českém jazyce.

Klíčová slova Replace with comma-separated list of keywords in Czech.

Abstract

The bachelor thesis focuses on utilizing LeapMotion sensors in realtime gesture recognition using artificial intelligence. We used two layered bidirectional LSTM architecture to classify static gestures along with dynamic gestures. The neural network was benchmarked on publicly available datasets and ultimately trained on handcrafted dataset used for realtime deployment of the trained model. We had created

Keywords Replace with comma-separated list of keywords in English.

Contents

Introduction	1
1 Neural Networks	3
1.1 Artificial Neuron	3
1.1.1 Perceptron	3
1.1.2 Sigmoid Neuron	4
1.1.3 Activation Function	4
1.1.3.1 Sigmoid Function	5
1.1.3.2 Hyperbolic Tangent	5
1.1.3.3 Rectified Linear Unit	6
1.1.3.4 Softmax	7
1.2 Types of Neural Networks	7
1.2.1 Feed-forward Networks	7
1.2.1.1 Cost Function	7
1.2.1.2 Backpropagation	8
1.2.2 Convolutional Neural Networks	8
1.2.2.1 Convolutional Layer	9
1.2.2.2 Pooling Layer	9
1.2.3 Recurrent Neural Networks	10
1.2.3.1 Bidirection Recurrent Neural Networks	11
1.2.4 Long Short-Term Memory	12
1.2.4.1 Bidirectional Long Short-Term Memory	14
1.2.4.2 Deep Long Short-Term Memory	15
2 Gesture Recognition	17
2.1 Gesture Categories	17
2.2 Tracking devices	17
2.2.1 Microsoft Kinect	18
2.2.2 Leap Motion Controller	18

2.2.3	Ultraleap Stereo IR 170	19
2.3	Gesture Recognition Methods	20
2.3.1	Static Gesture Recognition	20
2.3.2	Dynamic Gesture Recognition	21
2.3.3	Proposed LSTM solution	21
2.3.3.1	Feature Extraction	22
2.3.3.2	Optimal Number of Stacked LSTMs	23
2.3.3.3	Sampling Process	24
3	MultiLeap Library	27
3.1	Alignment of the tracking data	27
3.1.1	Data sampling	27
3.1.2	Kabsch algorithm	28
3.2	Data fusion	29
4	Implementation	31
4.1	Dataset Description	31
4.1.1	SHREC 2017 Dataset	31
4.1.2	ASL Dataset	31
4.1.3	Handicrafted Dataset	32
4.2	Model Training	34
4.2.1	DLSTM architecture	34
4.2.2	Two-Layered Bidirectional LSTM architecture	35
4.2.2.1	Selection of the Optimal Dropout Rate	35
4.2.2.2	Optimal number of stacked layers	35
4.3	Real-time recognition	37
4.3.1	Cppflow 2	37
4.3.2	Sliding window	37
5	Experiments	39
	Bibliography	41
A	Acronyms	47
B	Contents of enclosed CD	49

List of Figures

1.1	Perceptron [6]	4
1.2	Comparison between step function and sigmoid function	5
1.3	Hyperbolic tangent [6]	6
1.4	Rectified Linear Unit [6]	6
1.5	Fully connected Feed-forward Neural Network [6]	8
1.6	Convolution of an 5x5x1 image with 3x3x1 kernel [18]	9
1.7	Types of pooling [18]	10
1.8	Unrolled structure of RNN [6]	11
1.9	Unrolled structure of BRNN [6]	12
1.10	LSTM cell [26]	14
1.11	Unrolled structure of BLSTM [6]	14
1.12	Deep Long Short-Term memory architecture [28]	15
2.1	Azure Kinect [31]	18
2.2	Schematic View of Leap Motion Controller [33]	19
2.3	Leap Motion Controller Axes [34]	19
2.4	Schematic View of Ultraleap Stereo IR 170 [35]	20
2.5	Logical structure of the proposed method [30]	22
2.6	Internal angles of hand joints [30]	22
2.7	Model accuracy by using 800 epochs [30]	24
2.8	Model accuracy by using 1600 epochs for 5 LSTM layers and 1800 epochs for 6 LSTM layers [30]	24
2.9	Sampling example of feature ω_1	25
4.1	Train accuracies compared to validation accuracies through the course of learning	36
4.2	General idea of a sliding [51]	38

List of Tables

4.1	Average recognition accuracies across different depths of bidirectional lstm architectures using 5-fold on 200 epochs	36
-----	---	----

Introduction

Mouse and keyboard are considered to be default devices for human-computer interaction nowadays. But with the maturity in technology, namely virtual and extended reality, the computer's need to understand human's body language is more and more present. Actions such as rotation or grabbing and moving an object in three-dimensional space with a computer mouse are un-intuitive. They require a little understanding of the controls to execute the task. The movement is limited to the two-dimensional space of the mouse. Oppose to performing the desired action by hands in our three-dimensional space as we would in real life.

One of the proposed solutions for the issue is gesture recognition, where a general idea is for computers to have the ability to recognize gestures and perform actions based on them. Therefore, several devices, tracking devices, were developed to process an image and yield useful data for gesture recognition.

Our goal is to utilize these tracking devices, specifically Leap Motion controllers, combined with artificial neural networks, creating a simple library with a pre-trained model ready to be used and expanded by other applications. We also want to evaluate the recognition performance base on number of connected LMC sensors using MultiLeap library.

Neural Networks

An artificial neural network (ANN) is a mathematical model mimicking biological neural networks, namely their ability to learn and correct errors from previous experience [1], [2].

The ANN subject was first introduced by Warren McCulloch and Walter Pitts in "A logical calculus of the ideas immanent in nervous activity" published in 1943 [3]. But it was not until recent years when ANN has gained popularity with still increasing advancements in technology and availability of training data. ANN had become one of the default solutions for complex tasks which were previously thought to be unsolvable by computers [4].

This chapter will briefly explore different types of neural units and their activation functions, along with some exemplary network architectures.

1.1 Artificial Neuron

As previously mentioned, artificial neurons are units mimicking behavior of biological neurons. Meaning, it can receive as well as pass information between themselves.

1.1.1 Perceptron

Perceptron is the simplest class of artificial neurons developed by Frank Rosenblatt in 1958 [5].

Perceptron takes several binary inputs, vector $\vec{x} = (x_1, x_2, \dots, x_n)$, and outputs a single binary number. To express the importance of respected input edges, perceptron uses real numbers called *weights*, assigned to each edge, vector $\vec{w} = (w_1, w_2, \dots, w_n)$.

A *step function* calculates the perceptron's output. The function output is either 0 or 1 determined by whether its weighted sum $\alpha = \sum_i x_i w_i$ is less

or greater than its *threshold* value, a real number, usually represented as an incoming edge with a negative weight -1 [6].

$$output = \begin{cases} 1, & \text{if } \alpha \geq threshold \\ 0, & \text{if } \alpha < threshold \end{cases} \quad (1.1)$$

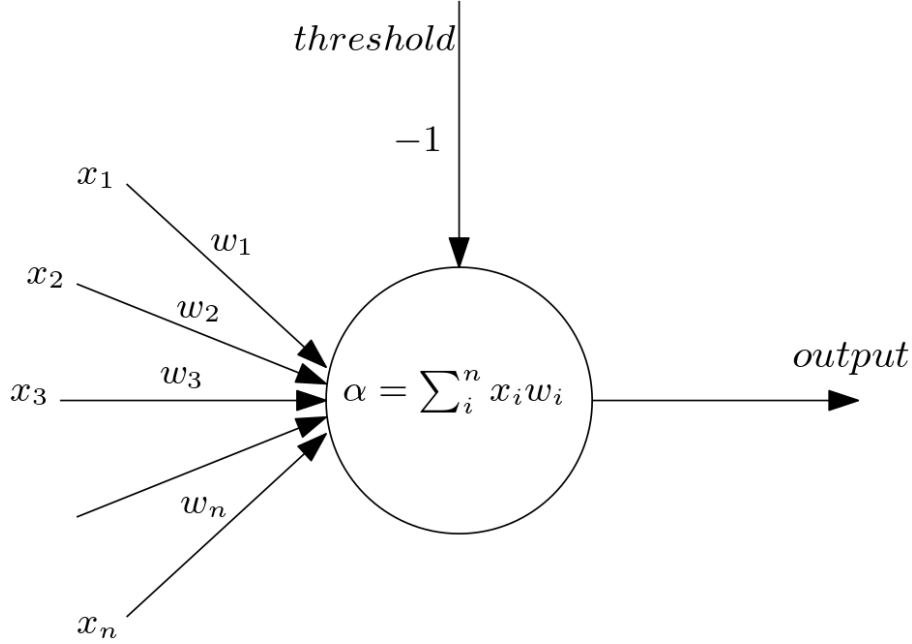


Figure 1.1: Perceptron [6]

1.1.2 Sigmoid Neuron

Sigmoid neuron, similarly to perceptron, has inputs \vec{x} and weights. The key difference comes in once we inspect the output value and its calculation. Instead of perceptron's binary output 0 or 1, a sigmoid neuron outputs a real number between 0 and 1 using a *sigmoid function* [7], [8], [6].

$$\sigma(\alpha) = \frac{1}{1 + e^{-\alpha}} \quad (1.2)$$

As shown in Figure 1.1, the sigmoid function(1.1a) is a smoothed-out version of the step function(1.1b).

1.1.3 Activation Function

An artificial neuron's activation function defines that neuron's output value for given inputs, commonly being $f : \mathbb{R} \rightarrow \mathbb{R}$ [9]. A significant trait of many activation functions is their differentiability, allowing them to be used for

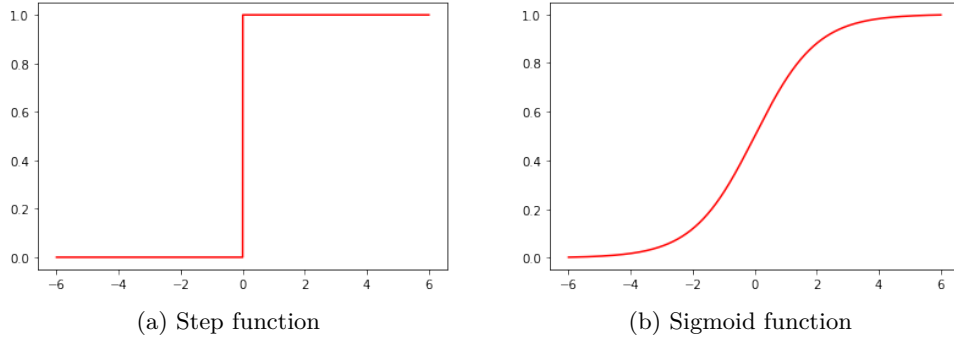


Figure 1.2: Comparison between step function and sigmoid function

Backpropagation, ANN algorithm for training weights. The activation function needs to have a derivative that does not saturate by heading towards 0, or explode by heading towards ∞ [6].

For such reasons, the usage of step function or any linear function is unsuitable for ANN.

1.1.3.1 Sigmoid Function

The sigmoid function is commonly used in ANN as an alternative to the step function. A popular choice of the sigmoid function is a *logistic sigmoid*. Its output value is in the range of 0 and 1.

$$\sigma(\alpha) = \frac{1}{1 + e^{-\alpha}} = \frac{e^x}{1 + e^x} \quad (1.3)$$

One of the reasons for its popularity is the simplicity of its derivative calculation:

$$\frac{d}{dx} \sigma(\alpha) = \frac{e^x}{(1 + e^x)^2} = \sigma(x)(1 - \sigma(x)) \quad (1.4)$$

On the other hand one of its disadvantages is the *vanishing gradient*. A problem where for a given very high or very low input values, there would be almost no change in its prediction. Possibly resulting in training complications or performance issues [10], [6].

1.1.3.2 Hyperbolic Tangent

Hyperbolic tangent is similar to logistic sigmoid function with a key difference in its output, ranging between -1 and 1.

$$\tanh(x) = \frac{e^x - e^{-x}}{e^x + e^{-x}} \quad (1.5)$$

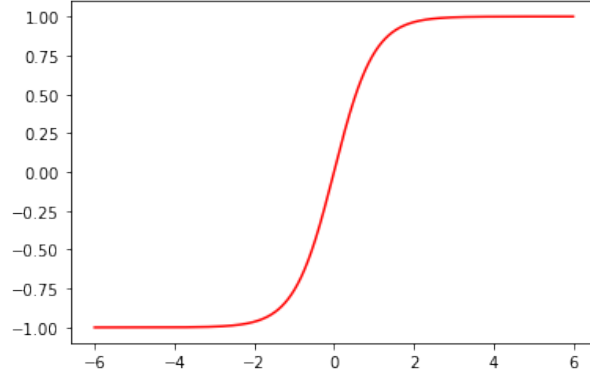


Figure 1.3: Hyperbolic tangent [6]

It shares sigmoid's simple calculation of its derivative.

$$\frac{d}{dx} \tanh(x) = 1 - \frac{(e^x - e^{-x})^2}{(e^x + e^{-x})^2} = 1 - \tanh^2(x) \quad (1.6)$$

By being only moved and scaled version of the sigmoid function, hyperbolic tangent does share sigmoid's advantages but also its disadvantages [9], [6].

1.1.3.3 Rectified Linear Unit

The output of the rectified linear unit (ReLU) is defined as:

$$f(x) = \max(0, x) \begin{cases} x, & \text{if } x \geq 0 \\ 0, & \text{if } x < 0 \end{cases} \quad (1.7)$$

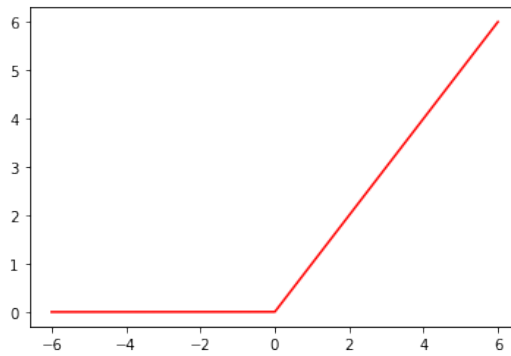


Figure 1.4: Rectified Linear Unit [6]

ReLU's popularity is mainly due to its computational efficiency [10]. Its disadvantages appear when inputs approach zero to or are negative number. Causing the so-called dying ReLU problem, where the network is unable to

learn. There are many variations of ReLU to this date, e.g., Leaky ReLU, Parametric ReLU, ELU, ...

1.1.3.4 Softmax

Softmax separates itself from all the previously mentioned functions by its ability to handle multiple input values in the form of a vector $\vec{x} = (x_1, x_2, \dots, x_n)$ and output for each x_i defined as:

$$\sigma(x_i) = \frac{e^{x_i}}{\sum_{j=1}^n e^{x_j}} \quad (1.8)$$

For output being normalized probability distribution, ensuring $\sum_i \sigma(x_i) = 1$ [11]. It is being used as the last activation function of ANN to normalize the network's output into n probability groups.

1.2 Types of Neural Networks

To this day, there are many types and variations of ANN, each with its structure and use cases. Here we will briefly introduce the most common ones, such as feed-forward networks, convolutional neural networks, or recurrent neural networks.

1.2.1 Feed-forward Networks

Feed-forward network (FFN) was the first ANN to be invented and the simplest form of ANN. Its name comes from the way how the information flows through the network. Its data travels in one direction, oriented from the *input layer* to the *output layer*, without cycles. The input layer takes input data, vector \vec{x} , producing \hat{y} at the output layer [12].

FFN may or may not contain several hidden layers of various widths. By having no back-loops, FFN generally minimizes error, computed by *cost function*, in its prediction by using the *backpropagation* algorithm to update its weight values [13], [11].

1.2.1.1 Cost Function

Cost function $C(\vec{w})$ is used in ANN's training process. It takes all weights and biases of an ANN as its input, in the form of a vector \vec{w} and calculates a single real number expressing ANN's incorrectness [14]. The number is high when the ANN performs poorly and gets lower when the ANN's output gets closer to the correct result. The main goal of training is then to minimize the cost function.

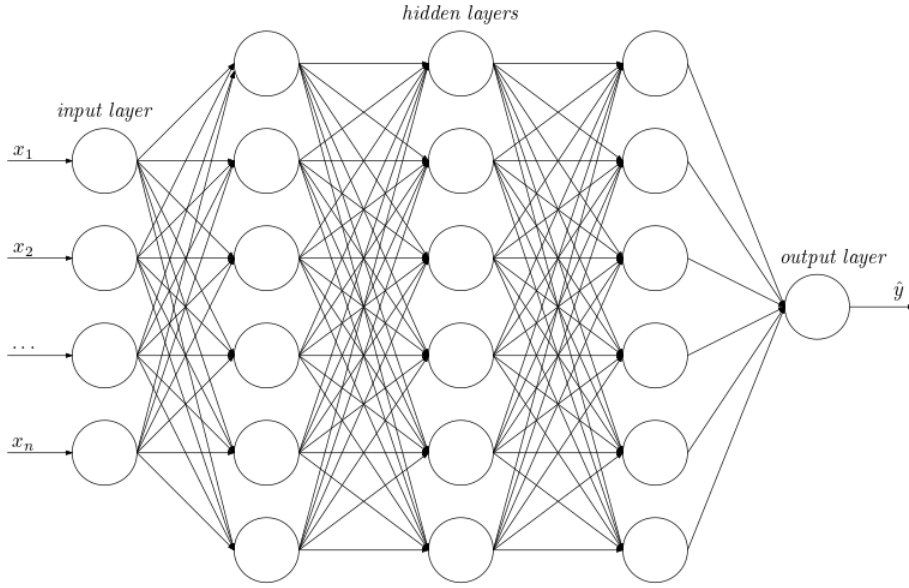


Figure 1.5: Fully connected Feed-forward Neural Network [6]

1.2.1.2 Backpropagation

Backpropagation, short of backward propagation of errors, is a widely used algorithm in training FFN using *gradient descent* to find a local minimum of a cost function and update ANN's weights [15].

A gradient of a function with multiple variables gives us the direction of the steepest gradient ascent, where should we step to increase the output quickly and find the local maximum. Naturally, its negative will point towards a local minimum.

The usual practice is to divide training samples into small *batches* of size n . We will calculate a gradient descent for each sample in the batch and use their average gradient descent to update the network's weights. The average gradient descent tells us which weights should be adjusted for the ANN to get closer to the correct results [15].

$$-\gamma \nabla C(\vec{w}_i) + \vec{w}_i \rightarrow \vec{w}_{i+1} \quad (1.9)$$

Here, \vec{w}_i are weights of the network at the current state (batch), \vec{w}_{i+1} are updated weights, γ is the learning rate and $-\nabla C(\vec{w}_i)$ is the gradient descent.

1.2.2 Convolutional Neural Networks

Convolutional Neural network's (CNN) main goal is to make a computer recognize images and objects. For such, it is primarily used for image classification or object recognition.

CNN was inspired by the biological processes of the human brain. Its connectivity patterns resemble the human's visual cortex. But an image is perceived differently by a human brain than by a computer. To a computer, an image is interpreted as an array of numbers. Thus CNN is designed to work with two-dimensional image arrays, although it is possible to work with one-dimensional or three-dimensional arrays too [16].

CNN is a variation of FNN [14]. It usually consists of the input layer followed by multiple hidden layers, typically several *convolutional layers* with standard *pooling layers*, and ending with the output layer.

1.2.2.1 Convolutional Layer

The convolutional layer's objective is to extract key features from the input image by passing a matrix known as a *kernel* over the input image abstracted into a matrix [17].

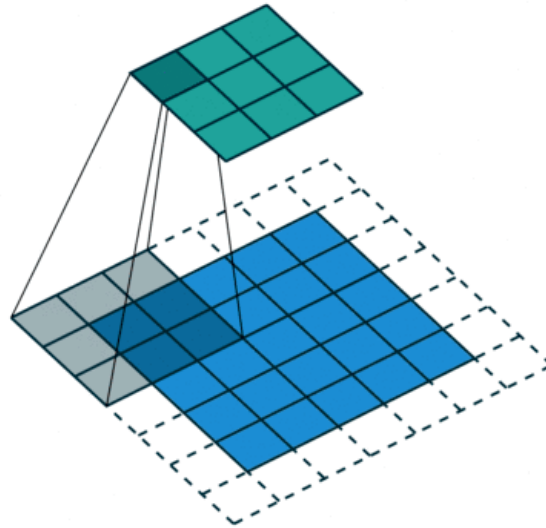


Figure 1.6: Convolution of an 5x5x1 image with 3x3x1 kernel [18]

The convolution result can be of two types depending on their size. One being the convolved feature is reduced in dimensions compared to the input, *valid padding*. For example, an input image of dimensions 8x8 being reduced to 6x6 after convolution operation, and the other type being where dimensions are either increased or remain the same, *same padding* [18].

1.2.2.2 Pooling Layer

Similar to the previously mentioned convolutional layer, the pooling layer reduces the convolved feature's spatial size to decrease the computational power

required for data processing. Furthermore, being useful by extracting dominant features, which are rotational and positional invariant, thus maintaining the process of effectively training the model [18].

There are two types of pooling: *max pooling* and *average pooling*. Max pooling returns the maximum value from the portion of the image covered by the kernel. It performs as a noise suppressant, discarding the noisy activations altogether and performing de-noising and dimensionality reduction. Where average pooling returns the average of all the values from the same covered portion, performing dimensionality reduction as a noise suppressing mechanism. Hence, it is possible to note that max-pooling performs better [18].

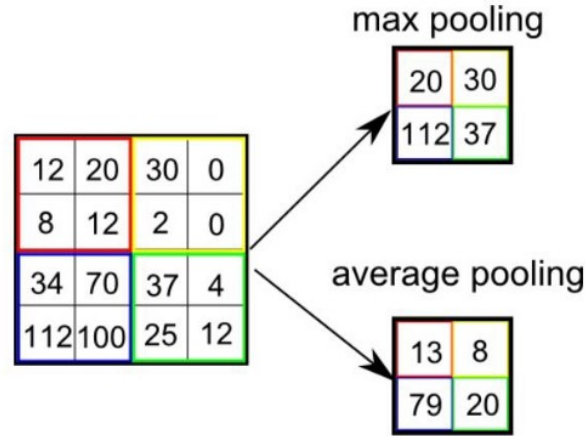


Figure 1.7: Types of pooling [18]

1.2.3 Recurrent Neural Networks

Recurrent Neural Network (RNN) is distinct by its memory, taking input sequence with no predetermined size. Its past predictions influence currently generated output. Thus for the same input, RNN could produce different results depending on previous inputs in the sequence [19].

RNNs features make it commonly used in fields such as speech recognition, image captioning, natural language processing, or language translation. Some of the popular being, for example, Siri, Google Translate or Google Voice search [20].

As previously mentioned, RNN takes into consideration information from previous inputs. Let us look at the idiom "feeling under the weather", where for it to make sense, words have to be in a specific order. RNN needs to account for each word's positions and use its information to predict the next word in the sequence. Each timestep represents a single word. In our case, the

third timestep represents "the". Its hidden state holds information of previous inputs, "feeling" and "under" [20].

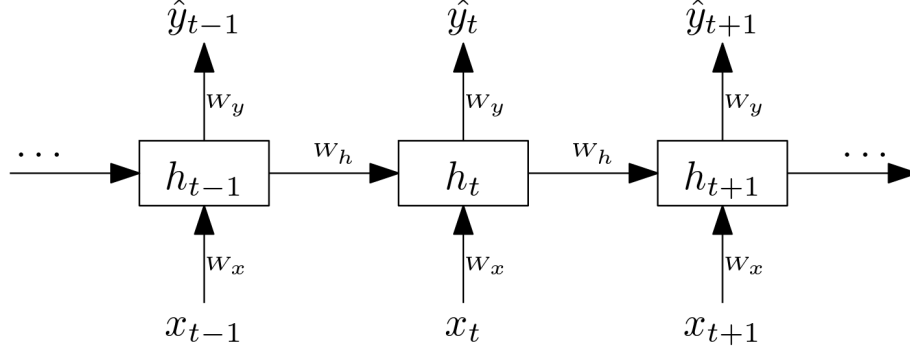


Figure 1.8: Unrolled structure of RNN [6]

Figure 1.8 shows the network for each timestep, i.e., at time t , the input \vec{x}_t goes into the network to produce output \hat{y}_t , the next timestep of the input is x_{t+1} with additional input from the previous time step from the hidden state h_t . This way, the neural network looks at the current input and has the context from the previous inputs. With this structure, recurrent units hold the past values, referred to as memory. Making it possible to work with a context in the data [21].

The recurrent unit is calculated as follows:

$$h_t = f(W_x x_t + W_h h_{t-1} + \vec{b}_h) \quad (1.10)$$

$f()$ being the activation function, W_x, W_h are weight matrixes, x_t is the input, and \vec{b}_h is the vector of bias parameters. Unit at time step $t = 0$ is initialized to $(0, 0, \dots, 0)$. The output \hat{y}_t is then calculated as:

$$\hat{y}_t = g(W_y h_t + \vec{b}_y) \quad (1.11)$$

$g()$ also being an activation function, usually being softmax to ensure the output is in the desired class range. W_y is the weight matrix and \vec{b}_y being a vector of biases determined during the learning process.

Training RNNs uses a modified version of the backpropagation algorithm called *backpropagation through time* (BPTT), working by unrolling the RNN [14], calculating the losses across time steps, then updating the weights with the backpropagation algorithm. More on RNN in [11] by Lipton et al.

1.2.3.1 Bidirection Recurrent Neural Networks

Bidirectional Recurrent Neural Networks (BRNN) allow training the network using all available input information in the past and future of a specific time frame. Oppose to regular RNN, where its hidden state is determined only by

the prior states. The idea behind BRNN is splitting the hidden state into two. One is responsible for the positive time direction, *forward states*, and the other for the negative time direction, *backward states*.

BRNN's training generally starts with processing forward, and backward states before output neurons are passed, *forward pass*. Following with *backward pass*, where output neurons are processed first, and forward and backward states after. Weights are then updated after completing forward pass and backward pass [22].

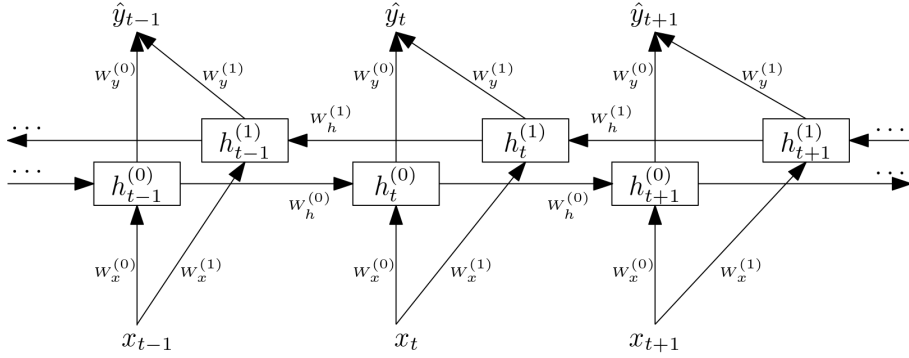


Figure 1.9: Unrolled structure of BRNN [6]

Both hidden states are updated identically as the hidden state in RNN.

$$h_t^{(0)} = f(W_x^{(0)}x_t + W_h^{(0)}h_{t-1} + \vec{b}_{h^{(0)}}) \quad (1.12)$$

$$h_t^{(1)} = f(W_x^{(1)}x_t + W_h^{(1)}h_{t-1} + \vec{b}_{h^{(1)}}) \quad (1.13)$$

The output is then computed in combination of both hidden states.

$$\hat{y}_t = g(W_y^{(0)}h_t^{(0)} + W_y^{(1)}h_t^{(1)} + \vec{b}_y) \quad (1.14)$$

All the activation functions and parameters remain the same as they were in RNN.

1.2.4 Long Short-Term Memory

Consider a task where we are trying to predict the last word in "The clouds are in the *sky*". It is fairly obvious the last word is meant to be "*sky*". The gap between the relevant information and the prediction place is small, and RNN can learn to utilize past information and predict the last word. However, if we consider "I grew up in Spain... I speak fluent *Spanish*", the gap between the relevant information and predicting word can become large. As the gap grows, RNNs are unable to handle the task. Such problem is called *long-term dependencies* [23].

Long Short Term Memory networks (LSTM) are RNN architecture first introduced by Hochreiter S. and Schmidhuber J. [24] with the ability to handle long-term dependencies. Its core idea is to replace RNN's hidden states with so-called **LSTM Cells** and add connections between cells, called cell states or c_t . Each LSTM Cell consists of three gates, regulating the input and output of the cell. The calculation in each cell runs as follows:

1. **Forget Gate:** Controls which information should be discarded and which kept. *Sigmoid function* outputs a value between 0 and 1 base on the information from the previous hidden state and from the current input. The value closer to 0 means discard, and closer to 1 means keep.

$$f_t = \sigma(W_{x_f}x_t + W_{h_f}h_{t-1} + \vec{b}_f) \quad (1.15)$$

2. **Input Gate:** Decides which information should be updated. The sigmoid function outputs a value between 0 and 1 base on the previous hidden state and current input state. Closer to 0 means not important, and closer to 1 means important.

$$i_t = \sigma(W_{x_i}x_t + W_{h_i}h_{t-1} + \vec{b}_i) \quad (1.16)$$

The information from the previous hidden state and current input state is also passed into a *tanh function*, getting values between -1 and 1.

$$g_t = \tanh(W_{x_g}x_t + W_{h_g}h_{t-1} + \vec{b}_g) \quad (1.17)$$

The decision on how to update the cell is obtained by multiplying sigmoid output and tanh output. With all the required values available, we can now calculate the **cell state** as follows:

$$c_t = i_t \odot g_t + f_t \odot c_{t-1} \quad (1.18)$$

3. **Output Gate:** Determines what information should the next hidden state contain. The previous hidden state and the current input are passed into a sigmoid function.

$$o_t = \sigma(W_{x_o}x_t + W_{h_o}h_{t-1} + \vec{b}_o) \quad (1.19)$$

Then passing the newly modified cell state into a tanh function, and multiplying its output with the sigmoid output, we get the hidden state [25].

$$h_t = o_t \odot \tanh(c_t) \quad (1.20)$$

The computation of the output \hat{y}_t proceeds the same way as regular RNN [6].

$$\hat{y}_t = g(W_y h_t + \vec{b}_y) \quad (1.21)$$

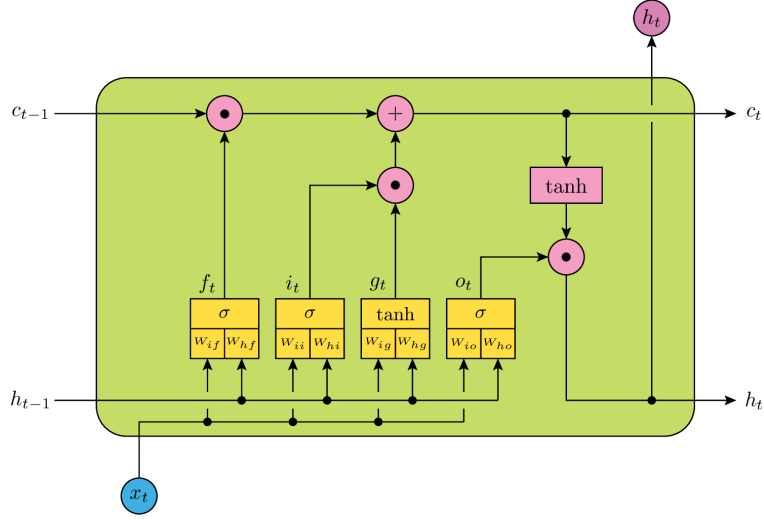


Figure 1.10: LSTM cell [26]

1.2.4.1 Bidirectional Long Short-Term Memory

Similarly, as previously described in BRNN (1.2.3.1), Bidirectional Long Short-Term Memory (BLSTM) has its hidden state split into two, forward states and backward states. Such modification allows the network to gain context from past and future alike. BLSTM, in comparison with BRNN, handles better the information storage across the timeline with large time gaps from either past or future.

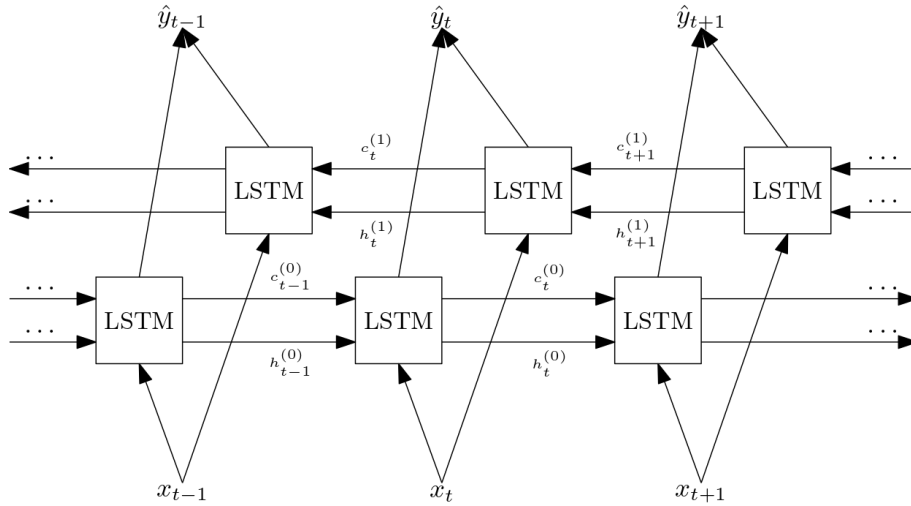


Figure 1.11: Unrolled structure of BLSTM [6]

1.2.4.2 Deep Long Short-Term Memory

Deep Long Short-Term Memory (DLSTM), or stacked LSTM, is now considered to be a stable technique for challenging sequence prediction tasks. It was first introduced by Graves, et al. [27], where it was found that the depth of the network has greater importance than the number of memory cells in a given layer. DLSTM architecture can be described as an LSTM model consisting of multiple LSTM layers.

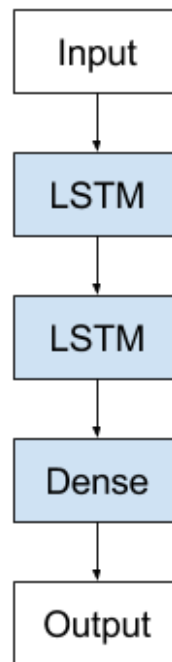


Figure 1.12: Deep Long Short-Term memory architecture [28]

The LSTM layer above outputs a sequence rather than a single value for the LSTM layer below [28].

Gesture Recognition

2.1 Gesture Categories

Gestures are categorized into *static gestures* and *dynamic gestures*. A Group of static gestures consists of fixed gestures, where they are not relative to time. A group of dynamic gestures, on the other hand, are time-varying. These classes can be further subdivided into a set of gestures distinct by their purpose.

- **Deictic gestures** involve pointing to establish the identity or spatial location of an object within the context of the application domain [29].
- **Manipulative gestures** mimic manipulation of a physical object, such as scaling, moving, or rotating.
- **Gesticulation** is commonly used along with the language group. These hand gestures are difficult to analyse.
- **Language group of hand gestures** form a grammatical structure for conversational style interfaces.
- **Semaphoric hand gestures** also may be referred to as communicative gestures, are a group of hand gestures serving as a set of symbols/commands used to interact with machines. The group consists of static hand gestures as well as dynamic hand gestures.

2.2 Tracking devices

Hand and body gesture recognition had followed a conventional scheme of extracting key features via one or multiple preprocessing sensors and applying machine learning techniques on them [30]. The field of gesture recognition gave birth to several image processing devices yielding useful data. We will

2. GESTURE RECOGNITION

only cover optical devices, but there are also controllers in the form of a stick with buttons, like HTC Vive, or others in the form of gloves, sending tracking information to the computer.

2.2.1 Microsoft Kinect

One of them being Microsoft Kinect, a device first released in 2010. Originally developed for gaming but eventually finding more success in academics and commercial applications, such as robotics, medicine, and health care, it led Microsoft to discontinue production of its Xbox version in 2018 and release Azure Kinect in March 2020, incorporating Microsoft Azure cloud computing functionalities.



Figure 2.1: Azure Kinect [31]

Azure Kinect contains a depth sensor, spatial microphone array with a video camera, and orientation sensor as a small all-in-one device with multiple modes, options, and software development kits [32].

With all that said, the primary purpose of the Kinect device overall is to interpret whole-body movement. For such, it lacks in required accuracy for hand gesture recognition, thus making it insufficient for our uses.

2.2.2 Leap Motion Controller

Another option would be using a Leap Motion Controller (LMC), developed specifically to track hand movements and extract its features, such as positions of fingers, hand rotation, and others.

LMC consists of two monochromatic IR cameras and three IR LEDs (emitters).

The LMC's current API, Leap Motion Service, yields positions of extracted hand features. All the positional data about the hand and its features are represented in the coordinate system relative to the LMC's center point, positioned at top of the controller [33]. The x- and z-axes lie in the camera sensors

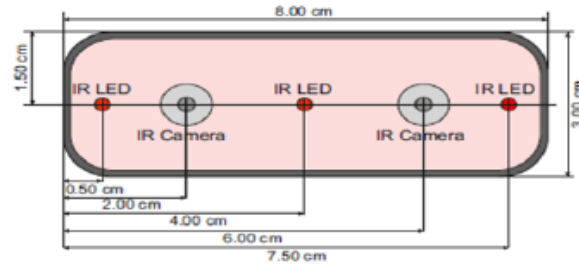


Figure 2.2: Schematic View of Leap Motion Controller [33]

plane, with the x-axis running along the camera baseline. The y-axis is vertical, with positive values increasing upwards (in contrast to the downward orientation of most computer graphics coordinate systems). The z-axis has positive values increasing toward the user [34].

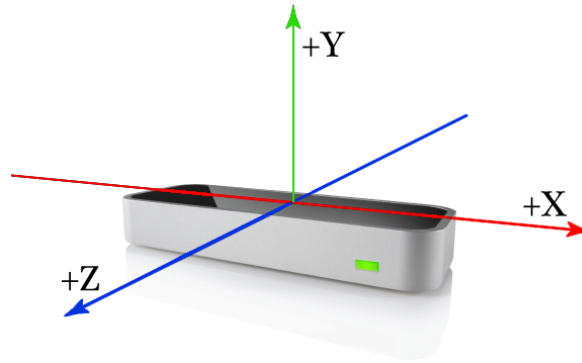


Figure 2.3: Leap Motion Controller Axes [34]

2.2.3 Ultraleap Stereo IR 170

Ultraleap Stereo IR 170, formerly known as the Leap Motion Rigel, is the successor to the Leap Motion controller.

The Stereo IR inherits Leap Motions key features but improves with a wider 170-degree field of view, more-powerful LED illuminators providing more extended tracking range, and a higher framerate when used with USB 3.0 [35], [36].

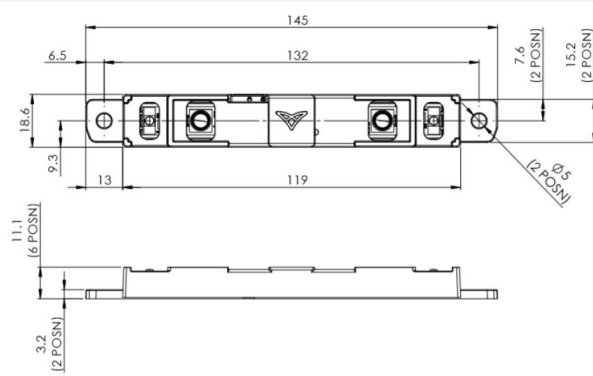


Figure 2.4: Schematic View of Ultraleap Stereo IR 170 [35]

Unfortunately, Leap Motion Controller, as well as Ultraleap Stereo IR 170, has no official library for gesture recognition, limiting developers from utilizing the controller for its key features. Leap Motion provided tracking software built for virtual reality, used to have a gesture detector with its 3.0 version, but the detector is absent with the release of more accurate version 4.0.

2.3 Gesture Recognition Methods

Gestures group classification should be taken into account when choosing appropriate methods due to their time-varying properties. As previously mentioned, gestures are classified into static and dynamic groups.

2.3.1 Static Gesture Recognition

One of the commonly used methods for static gesture recognition is *Support Vector Machine* (SVM), an algorithm used for both regression and classification tasks. But overall, it is widely used in classifications. SVM's goal is to find a *hyperplane* in N-dimension space, N being the number of features, that distinctively classifies data points [37]. *Hyperplanes* are decision boundaries between data points and optimal *hyperplane* is the one with maximal separation, *margin*, between classes [38].

Chen and Tseng [39] presented an SVM solution for multi-angle hand gesture recognition for rock paper scissors using images from a web camera. The training dataset consisted of 420 images and a testing set of 120 images. Datasets were collected from 5 different people for the right hand only and achieving 95%. The classifier still managed to recognize left-hand gestures with 90% accuracy.

Domino et al. [40] utilized SVM with Microsoft Kinect sensors. Extracting hand features, fingertips, and center of the hand, from the depth map and

feeding the data into SVM. Achieving 99.5% recognition rate on the dataset provided by Ren et al. [41]. The dataset consists of 10 different gestures performed by ten different people repeatedly each ten times, a total of 1000 different depth maps.

Mapari and Kharat [42] on the other hand, proposed a method to recognize American Sign Language (ASL) with an *Feed-forward network* using *Multilayer Perceptron (MLP)*, extracting data from LMC and computing 48 features (18 positional values, 15 distance values, and 15 angle values) for 4672 collected signs (146 users for 32 signs). The average classification accuracy is 90%.

2.3.2 Dynamic Gesture Recognition

Katia et al. [43] proposed a method classifying dynamic gestures acquired through LMC with a CNN. Adopting a modified version of ResNet-50 architecture, a 50 layers deep CNN, removing the last fully connected layer and adding a new layer with as many neurons as the considered collection of gesture classes. The acquired gesture information is converted into hand joints color images. The variation of hand joint positions during the gesture is projected on a plane, and temporal information is represented with the color intensity of the projected points. The trained model achieved 91% classification accuracy on the LMDHG dataset [44].

Ameur et al. [45] presented a solution using an SVM classifier used with LMC acquired data, (X, Y, Z) coordinates of fingertips and palm center. The experimental results show an accuracy of 81% on a dataset containing 11 actions, performed by ten different subjects, having in total 550 samples.

Yang L., Chen J., and Zhu W. [46] used two-layer Bidirectional RNN in combination with an LMC to classify dynamic hand gestures represented by sets of feature vectors (fingertip distance, angle, height, the angle of adjacent fingertips and the coordinates of the palm). The proposed method has been tested on the American Sign Language (ASL) datasets with 360 samples and the Handicraft-Gesture dataset with 480 samples, achieving 90% and 92% accuracy [46].

2.3.3 Proposed LSTM solution

Many of the proposed methods focus either on static gesture recognition or dynamic gesture recognition, but very few of them are actually utilized for both types at the same time.

Avola D., Bernardi M. et al. proposed a method in [30] utilizing LSTM, specifically Deep LSTM (DLSTM), and LMC to recognize sign language and semaphoric hand gestures. It uses a hand skeleton extracted by an LMC and considers angles formed by a specific subset of hand joints. The presented method reached 96% accuracy in its predictions.

2. GESTURE RECOGNITION

The LMC was used only to collect data for training. The method was not tested in real-time environment, it is yet to be explored whether it will.

Consider each hand gesture to be represented as set $X = \{x_0, x_1, \dots, x_{T-1}\}$ of feature vectors, in predetermined interval Θ size T , T being the number of time instances, in which features are extracted by LMC. DLSTM is applied to obtain series of output probability vectors $Y = \{y_0, y_1, \dots, y_{T-1}\}$. At last the gesture classification is performed by a *softmax* layer using $n = |C|$, where C being the set of considered hand gestures [30].

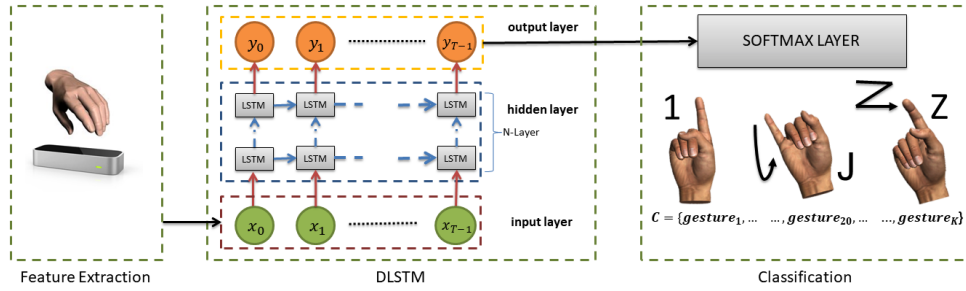


Figure 2.5: Logical structure of the proposed method [30]

2.3.3.1 Feature Extraction

A hand gesture can be considered to be composed of different poses, where particular angles characterize each pose. Each feature vector $x_t \in X$ consists mostly of internal angles, finger segments, palm position, and fingertip positions.

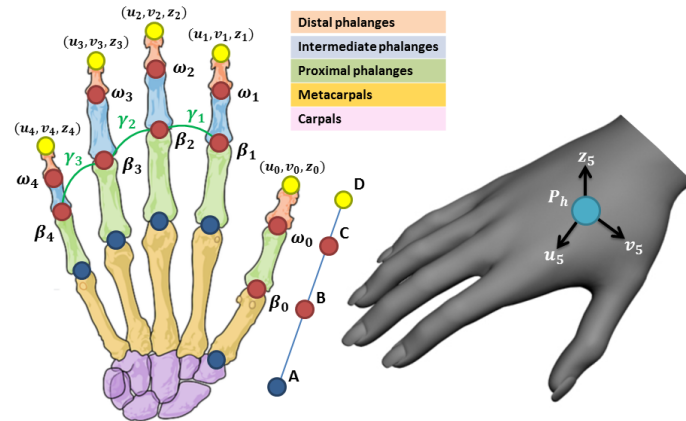


Figure 2.6: Internal angles of hand joints [30]

As seen in Figure 2.6, each finger can be represented as set of segments:

- \overline{AB} , proximal phalax, or metacarpal in case of thumb

- \overline{BC} , intermediate phalanx, or proximal phalanx in case of thumb
- \overline{CD} , distal phalanx

These set of segments are then used to calculate internal angles of considered finger:

- internal angles $\omega_1, \omega_2, \omega_3, \omega_4$ between distal phalanges and intermediate phalanges. Internal angle ω_0 of the thumb is calculated between distal phalanx and proximal phalanx.

$$\omega_{j \in \{0, \dots, 4\}} = \frac{\overline{BC} \cdot \overline{CD}}{|\overline{BC}| \cdot |\overline{CD}|} \quad (2.1)$$

- internal angles $\beta_1, \beta_2, \beta_3, \beta_4$ between intermediate phalanges and proximal phalanges. Internal angle β_0 of the thumb is calculated between proximal phalanx and metacarpal.

$$\beta_{j \in \{0, \dots, 4\}} = \frac{\overline{AB} \cdot \overline{BC}}{|\overline{AB}| \cdot |\overline{BC}|} \quad (2.2)$$

- intra-finger angles $\gamma_1, \gamma_2, \gamma_3$ are angles between two neighboring fingers, where considered fingers are: the pointer finger between middle finger, the middle finger and the ring finger, and the ring finger with a pinky finger. The infra-finger angles are used to handle special static gestures, for example, an open palm and a pop culture "Spock" greeting.

3D displacements of palm and fingertip positions serve to help classify dynamic hand gestures, where the movement is performed in 3D space.

- palm central point coordinates $P_h = (u_5, v_5, z_5)$ help to track the hand transition in the 3D space.
- finger tip positions $u_l, v_l, z_l, l \in 0, \dots, 4$ help to track the hand rotation in 3D space.

All above features form the input vector x_t passed to DLSTM at time t .

$$x_t = \{\omega_0, \dots, \omega_4, \beta_0, \dots, \beta_4, u_0, v_0, z_0, \dots, u_5, v_5, z_5, \gamma_1, \gamma_2, \gamma_3\} \quad (2.3)$$

2.3.3.2 Optimal Number of Stacked LSTMs

Several tests were performed to find the optimal number of stacked LSTMs. The results showed that having 4 LSTM layers proved to achieve the best accuracy by using 800 *epochs*, the number of times the learning algorithm goes through the complete training dataset. Although it was possible to get

2. GESTURE RECOGNITION

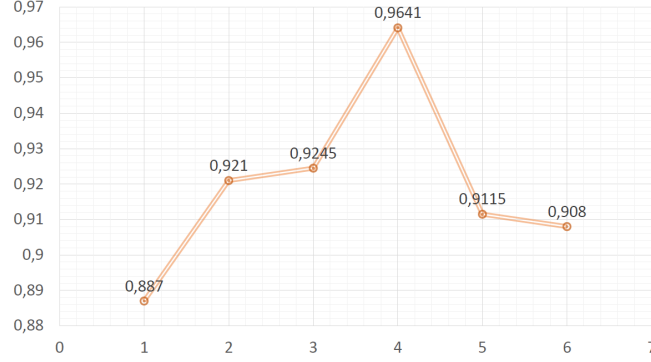


Figure 2.7: Model accuracy by using 800 epochs [30]

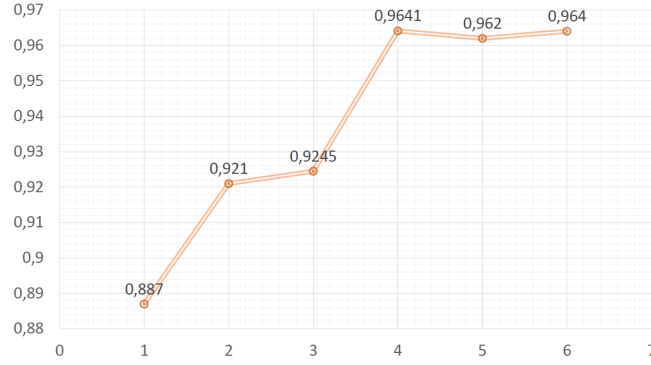


Figure 2.8: Model accuracy by using 1600 epochs for 5 LSTM layers and 1800 epochs for 6 LSTM layers [30]

the same results with 5 or 6 stacked LSTM layers, only due to using 1600 and 1800 epochs, thus increasing the training time [30].

The *learning rate* was set to 0.0001 after large empirical tests. The learning rate determines how much the newly acquired information about the weights will influence their updating. If the learning rate is too low, it will require more time to converge towards the local minimum, while if the rate is too large, it may overstep the local minimum [30].

2.3.3.3 Sampling Process

One gesture can be performed differently by each person, and all collected frame sequences must be composed of the same number of T samples. The proposed solution would collect data only in most significant T time instances, $t \in \Theta$ is considered significant if the joint angle and the central palm point coordinate P_h differs substantially between t and $t + 1$.

To explain more specifically, let $f_{\omega_i}(t)$, $f_{\beta_i}(t)$, $f_{\gamma_j}(t)$ be functions repre-

senting values of $\omega_i, \beta_i, \gamma_j$ angles at time t , where $0 \leq i \leq 4$ and $1 \leq j \leq 3$. Coordinates of P_h may be ϕ and coordinates at time t may be represented as $f_\phi(t)$. Then the Savitzky-Golay filter [47] is applied on each of the named functions, $f_g(t)$, $g \in G = \{\omega_i, \beta_i, \gamma_j, \phi\}$. Savitzky-Golay is a digital filter used to smooth a set of digital data in order to increase the signal-to-noise ratio without distorting the signal itself. Local extremes of each $f_g(t)$ are to be indentified as significant time variations and all time instances t , associated with at least one of these local maximum and minimum of feature g , form a new set Θ^* , representing candidates of possible important time instances to be sampled.

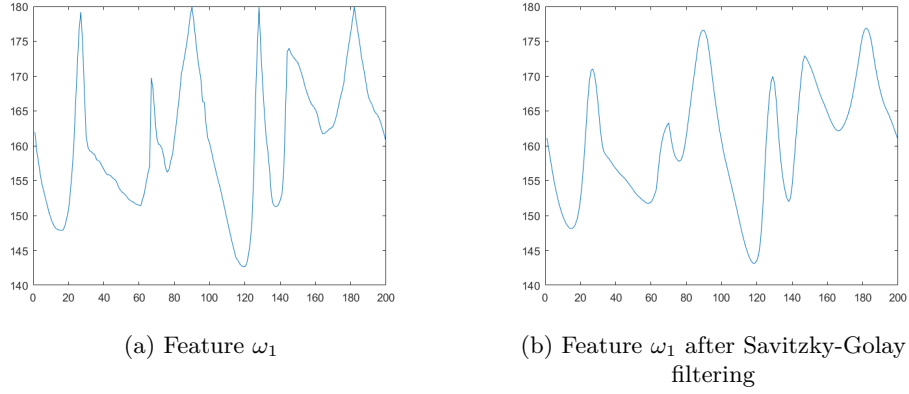


Figure 2.9: Sampling example of feature ω_1

Depending on the cardinality of the newly acquired set Θ^* , the following cases must be considered:

- $|\Theta^*| < T$, the remaining samples $(|\Theta^*| - T)$ are picked randomly from the original set Θ
- $|\Theta^*| > T$, only some of significant time instances for each g feature are picked to be sampled. Let $\Theta_g \subseteq \Theta^*$ be a set of significant time instances for feature g . The number of instances T_g to be sampled is chosen according to the ratio $|\Theta_g| : |\Theta^*| = T_g : T$, where the sum $\sum_{g \in G} T_g = T$ must be preserved [30].

MultiLeap Library

In 2018, developers from UltraLeap had released an experimental build for Leap Motion tracking software, which provided data from all connected LMCs at once. Despite having this feature, the provided tracking information for the same hand was different from each sensor due to different points of origin. This problem was solved by MultiLeap library created by Tomáš Nováček et al. in [34], which merges the information from all sensors and returns unified stream of data.

3.1 Alignment of the tracking data

To create tracking data alignment, we must first determine the position of LMCs, which can be achieved by data sampling or by accurate calculations of sensor's positions and rotations.

3.1.1 Data sampling

The MultiLeap library allows a user to sample data using a semi-automatic sampling process, which does not require the user to focus too much on the data acquisition itself.

The sampling is enabled manually, but data are sampled automatically per every Leap Motion frame, approximately 60 times per second. Each sample consists of 20 points from the hand – the points represent the center of each finger joint. The general idea of automatically sampling is to calibrate sensors using data from already calibrated devices. First, one sensor is marked as calibrated. The first marked sensor is either the first connected sensor or one selected by a user. Uncalibrated sensors start acquiring samples if the presented hand is in their field of view and at the same time in the field of view of any calibrated sensor. The sample consists of uncalibrated sensor's original data and fused data from all calibrated, to which is the hand visible. Once the sensor collects enough samples, it begins to compute the optimal translation

and rotation of the device. The sensor is then marked as calibrated. The process is repeated until all sensors are calibrated. [34]

Hands will then align automatically, but it is up to the user, performing the calibration, to cover enough space of the tracking area. Most importantly, it is best to have diverse data for more accurate alignment [34].

Considering the tracking data, where the hand is completely still, it will not have the necessary diversity in its samples. The deviation between collected tracking data is too insignificant. If we were to move the hand across the tracking area, having it rotated in various ways in various positions, the deviation of rotations and positions will be more evident, and the calculation of the alignment more precise [34].

Another option for calibration is a fully manual setting, which was already provided by Leap Motion Unity module, allowing a user to set the position and rotation of sensors in the Unity environment. Values need to be calculated accurately for the alignment to have any use. The main advantage of this approach is having the possibility of tracking different parts of the space with the sensors, for example, LMCs being back to each other.

The combined approach is also possible. First, making a rough calibration manually and eventually improved by the semi-automatic.

3.1.2 Kabsch algorithm

Kabsch algorithm [48] also known as Procrustes superimposition, was used to determine the rotation of sensors by calculating optimal rotation matrix minimizing the root mean squared deviation between two paired sets of points. The LMC sensor, selected by user, serves as a reference sensor and one of the considered sets. The second set of points consists of the tracking information from any other sensor. The algorithm is repeated for each connected sensor, excluding the reference sensor.

The goal of the Kabsch algorithm is to compute the optimal translation rotation of P onto Q, where P and Q are sets of pair points that minimize the distance between the two sets. Both P and Q are represented as $N \times 3$ matrix. Each row consists of coordinates of every point.

$$\begin{pmatrix} x_1 & y_1 & z_1 \\ x_2 & y_2 & z_2 \\ \vdots & \vdots & \vdots \\ x_N & y_N & z_N \end{pmatrix} \quad (3.1)$$

Coordinates of the first point are in the first row, the second point in the second row, and the Nth point in the Nth row.

The algorithm has two main steps, computing the optimal translation, computation of the optimal matrix.

The optimal translation can be easily found by being the offset between the averages of two sets of points. As for optimal rotation, we must first calculate the mean center of the points by subtracting the coordinates of the respective centroid from the point coordinates. The centroid C_P for P is computed as follows:

$$C_P = \frac{\sum_{i=1}^N P_i}{N} \quad (3.2)$$

The mean-center calculation of all points in P :

$$P_i = P_i - C_P \quad (3.3)$$

Then, the 3×3 cross-variance matrix between the points must be calculated as follows in matrix notation:

$$H = P^T Q \quad (3.4)$$

At last, we will extract the rotation from the covariance matrix using polar decomposition. The extraction can be done in more iterations, resulting in more accurate rotation calculation but requiring higher computation time in return.

3.2 Data fusion

If multiple sensors detect the hand, the fusion algorithm is used. In most cases, not all sensors detect the hands properly. One of the yield information provided by MultiLeap library is a *confidence*, a float value ranging from 0.3 to 1, which denotes the confidence level of the tracking data corresponding Leap Motion frame. The purpose of confidence level is to give more weight to tracking data from the sensor, which detects the hand better, making the tracking more accurate even if two out of three sensors would send inaccurate tracking data. The confidence level is of value 0.3 when the palm normal is in a 90° and 1 when in 0° or 180° angle to Y-axis. MultiLeap does not use the confidence of 0 because even with the occlusion of fingers and hand, the tracking data still carries some information about the hand. After few experiments, the value 0.3 was determined to be the most suitable confidence level for minimal tracking data when the palm normal is in 90° angle to the Y-axis of the sensor. The confidence is calculated by the following function, which transfers the angle, in radians, between the palm normal and the sensor's normal to the corresponding confidence level.

$$confidence = (0.283699 \cdot angle^2) - (0.891268 \cdot angle) + 1 \quad (3.5)$$

Implementation

As briefly mentioned in the Introduction chapter, our goal is to utilize Leap Motion controllers combined with the pre-trained ANN model. In the following chapter, we will explore datasets used for our training and the obstacles that came along with them. Then we will discuss the model training itself and its results. At last, we will deploy the trained model for real-time recognition in a C++ environment.

4.1 Dataset Description

Among many publicly available datasets for gesture recognition are only a few containing necessary skeletal information similar to those yield by Leap Motion controllers. We have selected ASL Dataset and SHREC 2017 Dataset created in conjunction with [30] and [49] respectively, often used as benchmark measurement for trained model accuracy.

4.1.1 SHREC 2017 Dataset

The SHREC dataset contains sequences of 14 dynamic hand gestures. Each gesture was performed between 1 and 10 times by 28 participants in two ways, using one finger and the whole hand. All participants were right-handed. The length of sample gestures varies between 20 to 170 frames, making some samples too short. The variation of frames makes it too inconsistent for our usage in real-time deployment and for such unsuitable.

4.1.2 ASL Dataset

ASL Dataset consists of 30 hand gestures, 18 static gestures, and 12 dynamic gestures. Gestures were collected from 20 different people. 13 were used to form the training set, while the remaining 7 formed a test set. Each person performed 30 hand gestures twice, once for each hand, and each gesture is

composed of fixed 200 frames as oppose to frame varying SHREC dataset [30].

After further inspection of the ASL dataset, we have discovered possible mislabeling of features. Specifically, taking a look at internal angles of gesture for number 1, we can see that 1 requires the ring finger to straighten out instead of the index finger. The same can be said about the gesture of number 2, where it appears to have the ring finger and middle finger straight out instead of the index finger and middle finger. It is unclear whether there are other mislabeling among the features. The mislabeling in itself is not an obstacle for training because the features are independent of each other, and the ANN can still learn on them, but the issue will arise in real-time classification, where raw data must be preprocessed identically as the training data. We decided not to use ASL Dataset for our purposes but only to benchmark model architecture.

4.1.3 Handicrafted Dataset

By not using ASL Dataset we have lost a set of static gestures. Also, we want to have the ability to provide the training with our own sets of gestures and not to be bound only to those publicly available. For such purposes, we had created a simple interactive data sampler in the form of a console application.

The sampler saves each sample in .txt format, one line by timestep T , frame yield by LMC, each line containing a set of features. Features were selected and computed as previously described in section 2.3.3.1. The order of features in a line x_t , at time t is as follows.

$$x_t = \{\omega_0, \dots, \omega_4, \beta_0, \dots, \beta_4, u_0, v_0, z_0, \dots, u_5, v_5, z_5, \gamma_1, \gamma_2, \gamma_3\} \quad (4.1)$$

All samples contain the same number of timesteps, specified at the beginning by the user or using default value of $T = 60$. The number of timesteps should be further analyzed inorder to find the optimal value. The value of timestep mostly affects the delay rate between presented gesture and its prediction in a real time environment, higher creates greater delay. Also, if the value is too high the dynamic gesture may have minimal role in the sample and we won't get desired behavior from our ANN. If the number is too low, the dynamic gesture may not be captured completely and the rate of performed predictions increases, creates greater demand on hardware.

The recording is initiated by key command, but the data collection does not start until the user's hand is in LMC's field of view. Data collection stops once the set of collected frames Θ matches T , or if the hand falls out of LMC's view. Features of missing timesteps are then set as zeroes. The sampling can be subdivided into 3 types:

1. **Single recording** records and saves a single sample. The next recording must be initiated by the user.

2. **Open recording** records and saves samples continuously. We recommend using the method only for static gestures. It is best to have a full control over recording a dynamic gesture, its beginning, and its end, along with its most significant sequence.
3. **Recording significant frames** records and saves a single sample. The next recording must be initiated by the user. The number of collected frames Θ^* is greater than the required number of timesteps $|\Theta^*| > T$. The last frame is excluded if $|\Theta^*|$ is not even. We will then calculate a *significance* between x_t and x_{t+1} . The *significance* of an interval is calculated as average euclidean distances of palm and finger tip positions P between x_t and x_{t+1} .

$$s_{(t,t+1)} = d(P_t, P_{t+1}) \quad (4.2)$$

$$S = \{s_{(0,1)}, \dots, s_{(t,t+1)}\} \quad (4.3)$$

Frames are then selected into Θ by most significant to least significant till $|\Theta| = T$. The following cases must be considered:

- $|\Theta| + 2 \leq T \wedge x_t$ and $x_{t+1} \notin \Theta$, both frames x_t and x_{t+1} will be added to Θ .
- $|\Theta| + 1 = T \wedge x_t$ and $x_{t+1} \notin \Theta$, both x_t and x_{t+1} are possible candidates for Θ but only one can be added due to the size $|\Theta|$ which would reach the limit after addition of one. In order to decide which to pick we will compare the significance $s_{(t-1,t)}$ and $s_{(t+1,t+2)}$, and pick greater of the two.
It is possible that x_t is the first frame of Θ^* , in which case we will pick x_{t+1} to be included in Θ . On the other hand, if x_{t+1} is the last frame of Θ^* , we will pick x_t .
- $x_t \notin \Theta \wedge x_{t+1} \in \Theta$, frame x_t is picked
- $x_t \in \Theta \wedge x_{t+1} \notin \Theta$, frame x_{t+1} is picked

The method is recommended for sampling dynamic gestures. We attempt to capture the most important part of a dynamic gesture, its movement. If the sampling is met with more delicate dynamic gestures performed only by fingers, it won't be able to underline the motion.

The most challenging part of creating a dataset is when we start the sampling itself. We want to keep in mind the variety of samples, meaning angles, positions and additionally when it comes to dynamic gestures, various speeds and starting positions. Also the factor of overlapping gestures must be taken into consideration.

Despite introducing sampling specifically for dynamic gestures, it can still be difficult to create a dataset, which will enforce the model to learn on characteristic movements. At the end, the trained model is just as good as the dataset it was trained on.

4.2 Model Training

We selected Python to be our primary language for training the ANN model along with the web-based interactive development environment Jupyter Notebook. One of the main reasons to pick Python over other available languages was its wide range of libraries and scientific packages supporting machine learning tasks. Most importantly, Keras, a high-level deep learning API integrated with TensorFlow, enabling the user to create and train model structures in very few steps.

SHREC Dataset and ASL Dataset were used to benchmark the model. For the purpose of real-time recognition, we trained the model on our handcrafted dataset consisting of numbers between 1 to 5 and simple dynamic gestures swipe left and right, where each gesture had 150 to 600 samples, 90 frames per sample, recorded in various angles, positions and speeds.

Each dataset was then split into 80% for the training set and 20% for the testing set, where 10% of the training set was used for validation. Each feature was then normalized via min-max scaler formula:

$$x' = \frac{x - \text{Min}(X)}{\text{Max}(X) - \text{Min}(X)} \quad x \in X \quad (4.4)$$

4.2.1 DLSTM architecture

At first, we followed the proposed architecture of 4 layers stacked LSTM by Avola D., Bernardi M. et al. [30]. We trained the model using 800 epochs and 0.0001 learning rate, which were proved to be optimal hyperparameters as described in section 2.3.3.2

Benchmarking the model on ASL Dataset resulted in similar accuracies as in [30]. Our handcrafted dataset had also achieved high results.

Despite achieving high accuracies on all datasets, the model itself did not perform well in a real-time environment. More specifically, the 4 layered LSTM architecture struggled with dynamic gestures. The model did not learn the gesture in relation to the movement but rather on its most occurring position in the recorded sequence, which in the case of swipe right was the palm's final position. The model successfully classified test samples because all gestures swipe right contained some frames where the palm position was on the right. Once we presented the model in a real-time environment with an open palm on the right, without the swipe movement, it classifies such gesture as swipe right, which is an undesired behavior.

It is unclear whether the model would perform better with more stacked LSTM layers or not, but we concluded that the architecture was not suitable for our purposes.

4.2.2 Two-Layered Bidirectional LSTM architecture

After an unsuccessful attempt to utilize DLSTM, we turned over to two-layered bidirectional LSTM architecture proposed in [46]. The proposed architecture was meant and trained on dynamic gestures only, not knowing how it will perform on static gestures. On the other hand, static gestures can be treated as a special type of dynamic gesture, having one frame stretched out to the desired number of timesteps. Not to mention our dataset was constructed in a way where static gestures have a slight difference in coordinates between t and $t + 1$, making it possible to look at the static gesture as a very slow type of dynamic gesture.

4.2.2.1 Selection of the Optimal Dropout Rate

To avoid the problem of overfitting, we used dropout regularization. A technique that, during training, randomly drops out a number of neurons in layers, thus ignoring their connections in the network. This creates a new smaller network and, in essence, simulates model ensembling without creating multiple networks.

We used ASL Dataset for its variety in samples and possible more complexity over our own handcrafted dataset. Despite its mislabeling of features, it still serves well for model benchmarking and validation.

The optimal dropout rate was selected through several experiments using dropout values in a range of 0.0 to 0.9. As seen below, not using dropout regulation caused a visible difference between train and validation accuracies through the course of training. The difference stayed poor, almost the same up to the value of 0.4, which showed improved results but not necessarily optimal. The difference was most promising when using dropout values of 0.5 and 0.6, where 0.6 performed better. However, the performance gets worse from 0.7 and on. The overall results indicate that the optimal dropout value is between 0.5 and 0.6. The value of 0.6 is satisfactory enough for our uses.

4.2.2.2 Optimal number of stacked layers

While searching for optimal dropout rate, we had performed the experiment across different depths of the network, more precisely 1 to 5 layered bidirectional LSTM networks. The dropout value appeared to have held the same characteristics for the different number of stacked layers.

The additional testing of the network's depth was to find out whether using a different number of layers than proposed in [46] would make any improvements in overall prediction performance.

4. IMPLEMENTATION

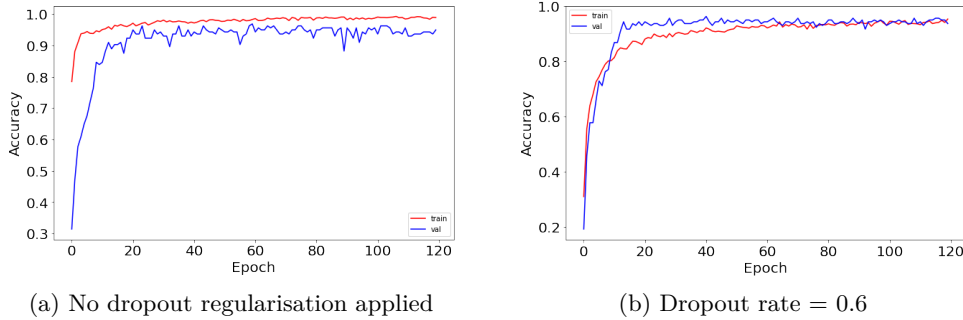


Figure 4.1: Train accuracies compared to validation accuracies through the course of learning

To find the optimal depth of the network, we have adopted k -fold Cross-validation. Cross-validation is often used to evaluate the performance of machine learning models on limited datasets. The entire data set is split randomly into k folds, in our case $k = 5$, then train the model using $k - 1$ folds and hold the remaining fold to measure the model’s accuracy. We will be repeating this process for each fold and then calculate the average performance across all folds.

Table 4.1: Average recognition accuracies across different depths of bidirectional lstm architectures using 5-fold on 200 epochs

<i>Number of layers</i>	<i>5-fold (%)</i>
1	88,14
2	89,07
3	87,48
4	86,31
5	87,98

The two-layered bidirectional LSTM architecture acquired the best performance results compared to other depths. Increasing the number of epochs would improve the results of architectures with more layers, but we would suffer on the side of the training time required. In conclusion, choosing the two-layered architecture is a good compromise between accuracy and training time.

The two-layered bidirectional LSTM architecture was successful in learning dynamic gestures base on its characteristic movement. It was also successful in classifying static gestures, both in real-time recognition.

4.3 Real-time recognition

The demo application for real-time recognition is in the form of a simple console application, supporting multiple LMCs using MultiLeap [34] library described in chapter 3 and with key commands for LMC calibration. When a hand gesture is presented, the application prints out the prediction, which is considered a valid prediction if the value passes the threshold of 90% accuracy. The demo application served mainly for debugging and experimental purposes.

For real-time recognition, we chose C++ as our primary language since C++ and C# are widely used programming languages in graphic engines such as Unity, PhyreEngine, or Unreal, which opens the possibility of integrating our application into graphic engines in future works.

4.3.1 Cppflow 2

Our application uses the trained model from section 4.2 and deploys it in C++ environment. More specifically, we exported the model in .tf file format and imported it into C++ using CppFlow 2.

Cppflow 2 is an API created by Sergio Izquierdo, allowing the user to run TensorFlow in C++ without the necessity of installing and compiling TensorFlow itself. CppFlow 2 serves as a Tensorflow C API wrapper providing a simple C++ interface similar to TensorFlow callings in Python environment [50].

4.3.2 Sliding window

The data collection, frame collection yield by LMC, starts once a hand is presented in LMC's field of view and stops if the hand falls out of the view. Let us introduce a situation where during the stream of data yield by LMC, we change our hand gesture from a "fist" to a "peace sign". We want to classify both of these gestures, but how do we determine where one gesture ends and the other starts. To tackle the presented scenario, we adopted the concept of *sliding window*.

The basic idea is to have a window of fixed size T , which slides through our data stream and captures a certain portion of it. It is important to remain the same T value as we chose to record our dataset. Otherwise, the shape of the captured data would differ from the input shape of our trained model. It is worth mentioning that using a wider window size creates a noticeable time delay between a presented gesture and its prediction. On the other hand, using a size too small, there would be a possibility of not capturing a dynamic gesture completely, leading to possible inaccurate predictions. In our case we used $T = 60$. Considering a situation where a collected data is less than T , the missing data are then set to zeroes. If we present more than one hand, the

4. IMPLEMENTATION

stream is invalidated, collected data are flushed, and the window will begin its sliding again once there is only one hand in the controller's view.

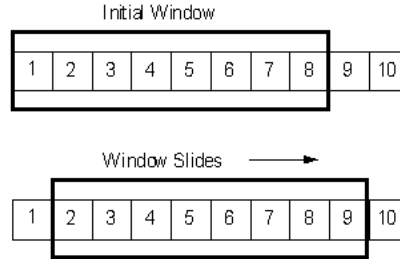


Figure 4.2: General idea of a sliding [51]

For each window, we then calculate features for classification and output the prediction of the captured portion. Features must be preprocessed exactly the same as they were for model training, in our case, same as described in section 2.3.3.1.

The window slides by ten frame, in other words throws away oldest frames and adds in newest acquired. The slide rate should be further tuned for optimal value. If we throw away too many frames, we risk of leaving some gestures unclassified. On the other hand, sliding by one frame can be demanding on hardware, where weaker computer builds may not be able to keep up and the prediction may stutter.

Experiments

As mentioned in Introduction chapter, we would also want to evaluate the recognition performance based on a number of connected LMC sensors. We mainly focused on the overall placement of sensors and their field of view., having a single connected sensor as a reference field of view and exploring its expansion using different layouts with a different number of connected sensors.

Bibliography

- [1] Chen, Y.-Y.; Lin, Y.-H.; et al. Design and Implementation of Cloud Analytics-Assisted Smart Power Meters Considering Advanced Artificial Intelligence as Edge Analytics in Demand-Side Management for Smart Homes. *Sensors*, 05 2019, doi:10.3390/s19092047.
- [2] Bengio, Y.; Goodfellow, I.; et al. *Deep learning*, volume 1. Citeseer, 2017, ISBN 0262035618, 166–485 pp.
- [3] McCulloch, W. S.; Pitts, W. A logical calculus of the ideas immanent in nervous activity. *The bulletin of mathematical biophysics*, volume 5, no. 4, 1943: pp. 115–133, ISSN 0007-4985.
- [4] Krishtopa. What Are Neural Networks, Why They Are So Popular And What Problems Can Solve. 2016. Available from: <https://steemit.com/academia/@krishtopa/what-are-neural-networks-why-they-are-so-popular-and-what-problems-can-solve>
- [5] Rosenblatt, F. The Perceptron: A Probabilistic Model For Information Storage And Organization In The Brain. *Psychological Re-view*, 1958: p. 2047, doi:0.1037/h0042519.
- [6] Kozák, M. Static malware detection using recurrent neural networks. [cit. 2020-12-28]. Available from: <https://dspace.cvut.cz/bitstream/handle/10467/88342/F8-BP-2020-Kozak-Matous-thesis.pdf?sequence=-1&isAllowed=y>
- [7] Nielsen, M. A. *Neural Networks and Deep Learning*. Determination Press, 2015.
- [8] Rojas, R. *Neural networks: a systematic introduction*. Springer Science & Business Media, 2013, ISBN 9783642610684, 37–99 pp.

- [9] Leskovec, J.; Rajaraman, A.; et al. *Mining of massive data sets*. Cambridge university press, 2020, ISBN 9781108476348, 523–569 pp.
- [10] Maladkar, A. I. M., Kishan. 6 Types of Artificial Neural Networks Currently Being Used in ML. [cit. 2020-12-25]. Available from: <https://analyticsindiamag.com/6-types-of-artificial-neural-networks-currently-being-used-in-todays-technology/>
- [11] Lipton, Z. C.; Berkowitz, J.; et al. A critical review of recurrent neural networks for sequence learning. *arXiv preprint arXiv:1506.00019*, 2015: pp. 5–25, ISSN 2331-8422. Available from: <https://arxiv.org/pdf/1506.00019.pdf>
- [12] Wiki, B. M. . S. Feedforward Neural Networks. [cit. 2020-12-25]. Available from: <https://brilliant.org/wiki/feedforward-neural-networks/>
- [13] Towards AI, M. Main Types of Neural Networks and its Applications-Tutorial. Aug 2020, [cit. 2020-12-25]. Available from: <https://medium.com/towards-artificial-intelligence/main-types-of-neural-networks-and-its-applications-tutorial-734480d7ec8e>
- [14] Goodfellow, I.; Bengio, Y.; et al. *Deep Learning*. MIT Press, 2016, url-<http://www.deeplearningbook.org>.
- [15] Wiki, B. M. . S. Backpropagation. [cit. 2020-12-25]. Available from: <https://brilliant.org/wiki/backpropagation/>
- [16] How Do Convolutional Layers Work in Deep Learning Neural Networks? April 2020, [cit. 2020-12-25]. Available from: <https://machinelearningmastery.com/convolutional-layers-for-deep-learning-neural-networks/>
- [17] MathWorks. Convolutional Neural Network. [cit. 2020-12-25]. Available from: <https://www.mathworks.com/solutions/deep-learning/convolutional-neural-network.html>
- [18] Science, T. D. A Comprehensive Guide to Convolutional Neural Networks-the ELI5 way. Dec 2018, [cit. 2020-12-25]. Available from: <https://towardsdatascience.com/a-comprehensive-guide-to-convolutional-neural-networks-the-eli5-way-3bd2b1164a53>
- [19] Science, T. D. Recurrent Neural Networks. Jun 2019, [cit. 2020-12-25]. Available from: <https://towardsdatascience.com/recurrent-neural-networks-d4642c9bc7ce>
- [20] IBM. What are Recurrent Neural Networks? [cit. 2020-12-25]. Available from: <https://www.ibm.com/cloud/learn/recurrent-neural-networks>

-
- [21] Medium. Understanding Recurrent Neural Networks in 6 Minutes. Sep 2019, [cit. 2020-12-25]. Available from: <https://medium.com/x8-the-ai-community/understanding-recurrent-neural-networks-in-6-minutes-967ab51b94fe>
- [22] Schuster, M.; Paliwal, K. Bidirectional recurrent neural networks. *Signal Processing, IEEE Transactions on*, volume 45, 12 1997: pp. 2673 – 2681, doi:10.1109/78.650093.
- [23] Olah, C. Understanding LSTM Networks [online]. [cit. 2020-12-28]. Available from: <https://colah.github.io/posts/2015-08-Understanding-LSTMs/>
- [24] Hochreiter, S.; Schmidhuber, J. Long Short-term Memory. *Neural computation*, volume 9, 12 1997: pp. 1735–80, doi:10.1162/neco.1997.9.8.1735.
- [25] Phi, M. Illustrated Guide to LSTM's and GRU's: A step by step explanation [online]. [cit. 2020-12-28]. Available from: <https://towardsdatascience.com/illustrated-guide-to-lstms-and-gru-s-a-step-by-step-explanation-44e9eb85bf21>
- [26] Holzner, A. LSTM cells in PyTorch [online]. Oct 2017, [cit. 2020-12-28]. Available from: <https://medium.com/@andre.holzner/lstm-cells-in-pytorch-fab924a78b1c>
- [27] Graves, A.; Mohamed, A.; et al. Speech Recognition with Deep Recurrent Neural Networks. *CoRR*, volume abs/1303.5778, 2013, 1303.5778. Available from: <http://arxiv.org/abs/1303.5778>
- [28] Brownlee, J. Stacked Long Short-Term Memory Networks [online]. Aug 2019, [cit. 2020-12-28]. Available from: <https://machinelearningmastery.com/stacked-long-short-term-memory-networks/>
- [29] Vafaei, F.; Slator, B.; et al. Taxonomy of Gestures in Human Computer Interaction. 12 2013.
- [30] Avola, D.; Bernardi, M.; et al. Exploiting Recurrent Neural Networks and Leap Motion Controller for the Recognition of Sign Language and Semaphore Hand Gestures. *IEEE Transactions on Multimedia*, volume 21, no. 1, Jan 2019: p. 234–245, ISSN 1941-0077, doi:10.1109/tmm.2018.2856094. Available from: <http://dx.doi.org/10.1109/TMM.2018.2856094>
- [31] Microsoft. Azure Kinect [online]. [cit. 2020-12-25]. Available from: <https://img-prod-cms-rt-microsoft-com.akamaized.net/cms/api/am/imageFileData/RWq0sq?ver=2e37>

- [32] Microsoft. Azure Kinect DK documentation [online]. [cit. 2020-12-25]. Available from: <https://docs.microsoft.com/en-us/azure/Kinect-dk/>
- [33] Weichert, F.; Bachmann, D.; et al. Analysis of the Accuracy and Robustness of the Leap Motion Controller. *Sensors (Basel, Switzerland)*, volume 13, 05 2013: pp. 6380–6393, doi:10.3390/s130506380.
- [34] Novacek, T.; Martin, C.; et al. Project MultiLeap: Fusing Data from Multiple Leap Motion Sensors. In *Proceedings of 2021 IEEE 7th International Conference on Virtual Reality (ICVR 2021)*, ICVR 2021, New York, NY, USA: IEEE, 2021, pp. 19–26.
- [35] Ultraleap. Tracking: Ultraleap Stereo IR 170 Evaluation Kit [online]. [cit. 2020-12-26]. Available from: <https://www.ultraleap.com/product/stereo-ir-170/>
- [36] Prototyping, S. Ultraleap Stereo IR 170 [online]. [cit. 2020-12-26]. Available from: <https://www.smart-prototyping.com/Ultraleap-Stereo-IR-170>
- [37] Microsoft. Support Vector Machine - Introduction to Machine Learning Algorithms [online]. 7 2018, [cit. 2020-12-25]. Available from: <https://towardsdatascience.com/support-vector-machine-introduction-to-machine-learning-algorithms-934a444fca47>
- [38] Alexandre Savaris, A. v. W. A. Comparative evaluation of static gesture recognition techniques based on nearest neighbor, neural networks and support vector machines. *J Braz Comput Soc*, volume 16, 2010: p. 147–162, doi:10.1007/s13173-010-0009-z.
- [39] Chen, Y.; Tseng, K. Developing a Multiple-angle Hand Gesture Recognition System for Human Machine Interactions. 2007: pp. 489–492, doi:10.1109/IECON.2007.4460049.
- [40] Dominio, F.; Donadeo, M.; et al. Hand Gesture Recognition with Depth Data. 2013: p. 9–16, doi:10.1145/2510650.2510651. Available from: <https://doi.org/10.1145/2510650.2510651>
- [41] Ren, Z.; Yuan, J.; et al. Robust hand gesture recognition based on finger-earth mover’s distance with a commodity depth camera. *MM’11 - Proceedings of the 2011 ACM Multimedia Conference and Co-located Workshops*, 11 2011: pp. 1093–1096, doi:10.1145/2072298.2071946.
- [42] Mapari, R. B.; Kharat, G. American Static Signs Recognition Using Leap Motion Sensor. 2016, doi:10.1145/2905055.2905125. Available from: <https://doi.org/10.1145/2905055.2905125>

-
- [43] Lupinetti, K.; Ranieri, A.; et al. 3D Dynamic Hand Gestures Recognition Using the Leap Motion Sensor and Convolutional Neural Networks. 2020: pp. 420–439.
- [44] Boulahia, S. Y.; Anquetil, E.; et al. Dynamic hand gesture recognition based on 3D pattern assembled trajectories. 2017: pp. 1–6, doi:10.1109/IPTA.2017.8310146.
- [45] Ameer, S.; Khalifa, A. B.; et al. A comprehensive leap motion database for hand gesture recognition. 2016: pp. 514–519, doi:10.1109/SETIT.2016.7939924.
- [46] Yang, L.; Chen, J.; et al. Dynamic Hand Gesture Recognition Based on a Leap Motion Controller and Two-Layer Bidirectional Recurrent Neural Network. *Sensors*, volume 20, 04 2020: p. 2106, doi:10.3390/s20072106.
- [47] Savitzky, A.; Golay, M. J. E. Smoothing and Differentiation of Data by Simplified Least Squares Procedures. *Anal. Chem.*, volume 36, no. 8, July 1964: pp. 1627–1639, doi:10.1021/ac60214a047. Available from: <http://dx.doi.org/10.1021/ac60214a047>
- [48] Kabsch, W. A solution for the best rotation to relate two sets of vectors. *Acta Crystallographica Section A*, volume 32, no. 5, Sep 1976: pp. 922–923, doi:10.1107/S0567739476001873. Available from: <https://doi.org/10.1107/S0567739476001873>
- [49] De Smedt, Q.; Wannous, H.; et al. SHREC’17 Track: 3D Hand Gesture Recognition Using a Depth and Skeletal Dataset. Apr. 2017: pp. 1–6, doi:10.2312/3dor.20171049. Available from: <https://hal.archives-ouvertes.fr/hal-01563505>
- [50] Izquierdo, S. CppFlow 2 [online]. [cit. 2021-3-18]. Available from: <https://github.com/serizba/cppflow>
- [51] Sliding window protocol [online]. [cit. 2021-06-12]. Available from: <https://www.toppr.com/ask/question/sliding-window-protocol-have/>

Acronyms

GUI Graphical user interface

XML Extensible markup language

Contents of enclosed CD

	readme.txt.....	the file with CD contents description
	exe	the directory with executables
	src.....	the directory of source codes
	wbdcm	implementation sources
	thesis.....	the directory of \LaTeX source codes of the thesis
	text	the thesis text directory
	thesis.pdf	the thesis text in PDF format
	thesis.ps	the thesis text in PS format